Research on Chemical Intermediates (2025) 51:633–655
https://doi.org/10.1007/s11164-024-05481-5

Silver salts of 12-tungstophosphoric acid supported on SBA-15: effect of enhanced specific surface area on ethanol dehydration

Mayara A. Resende[1] · Maria Clara Hortencio Clemente[1] · Gesley Alex Veloso Martins[1] · Luís Carlos Cides da Silva[2] · Marcia C. A. Fantini[2] · Sílvia C. L. Dias[1] · José A. Dias[1]

Received: 20 October 2024 / Accepted: 12 December 2024 / Published online: 6 January 2025

Abstract

This work reports the preparation, characterization, and application of silver salt derivatives of HPW (Ag_xHPW) in ethanol dehydration. The materials were fully characterized by elemental EDXRF analysis, XRD, SAXS, SEM, FT-IR, ^{31}P MAS NMR, thermal analysis (TG/DTG), N_2 sorption at low temperature (− 196 °C), and pyridine adsorption acidity. The results of the characterization demonstrated that the Keggin structure was preserved in all the synthesized materials. Using the ethanol dehydration model reaction, it was possible to select the most active catalyst in the series: Ag_2HPW. Activation of this salt at 200 and 300 °C revealed that the degree of hydration is an important parameter for catalytic activity. In addition, a dependence on the BET specific surface area was detected for both conversion and selectivity towards ethylene in the salt series. The conversion of ethanol was significantly enhanced after loading 20 wt.% of Ag_2HPW onto ordered mesoporous silica type SBA-15. The reaction conditions were optimized, and the best catalyst (20%Ag_2HPW/SBA-15, calcined at 300 °C) achieved complete ethanol conversion with about 100% selectivity towards ethylene at a temperature of 400 °C.

Extended author information available on the last page of the article

Graphical abstract

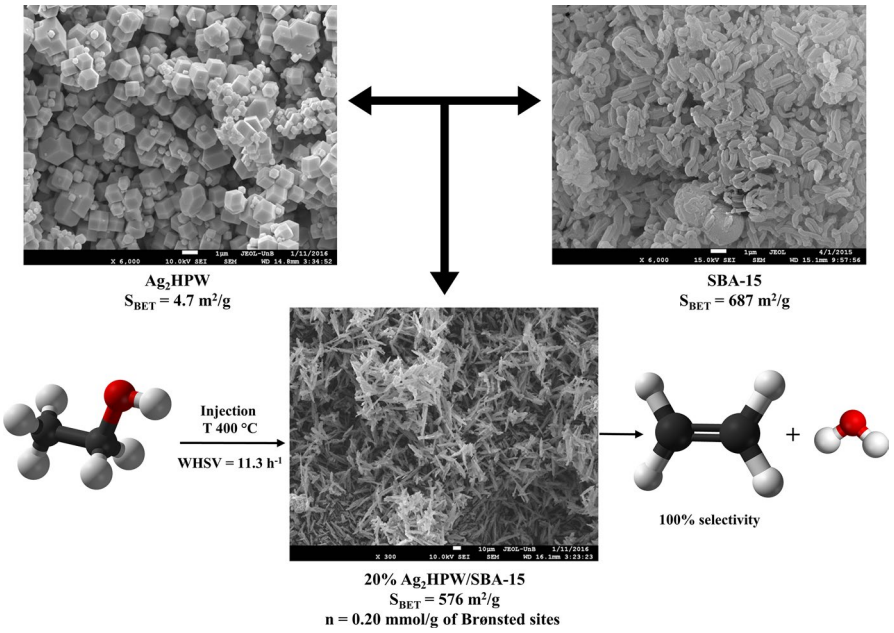

Keywords 12-tungstofosphoric acid · Silver salts of 12-tungstofosphoric acid · SBA-15 · Composite 20%AgxHPW/SBA-15 · Ethanol dehydration · Ethylene

Introduction

Polyoxometalates, specifically heteropolyacids (HPAs) with Keggin structures, such as 12-tungstophosphoric acid ($H_3PW_{12}O_{40}$, HPW), have been extensively studied for catalytic applications due to the following properties: strong acidity, redox ability, and good thermal stability. However, their main disadvantages are very low surface area (< 5 m2 g¯1) and high solubility in water and polar solvents when applied in heterogeneous catalysis [1]. Several alternatives have been proposed in the literature to overcome these issues: (i) partial or total replacement of HPW protons by cations, forming insoluble salts; (ii) partial replacement of the addenda atoms (e.g., Mo(VI) or W(VI) by V(V), Ti(IV)); and (iii) preparation of different HPAs supported on high specific surface area matrices [1–4]. HPW exhibits structural flexibility that enables ion exchange without fragmentation of the Keggin anion. $Ag_xH_{(3-x)}PW_{12}O_{40}$ (Ag_xHPW) derivatives of HPW have attracted great interest due to their multifunctional activities [2]. The HPW silver salt derivatives have shown significant acidity, measured by ammonia sorption, which is considered to be about an order of magnitude higher than that of cesium salt derivatives of HPW [5]. This high acidity is

assumed to be produced by the dissociation of the water molecules coordinated to the silver cations [6, 7].

The SBA-15 (Santa Barbara Amorphous-15) type of ordered mesoporous silica (OMS) is a material with uniform micro- and mesoporosity, which can be tailored by synthetic experimental conditions [8–10]. This material exhibits a series of promising properties for use as a support, such as high specific surface area, a hexagonal structure of highly ordered pores, and remarkable thermal stability [8–11]. The use of SBA-15 to support nanoparticles of HPA is an alternative for achieving a significant increase in specific surface area and better accessibility of the substrate to the catalytic active centers. For instance, the HPA amino-functionalized molecular sieve catalysts demonstrated significantly improved oxidation catalytic activity (acetaldehyde formation) and reduced acid catalytic activity (ethylene and diethyl ether formation) in comparison to the unsupported catalyst [12].

The production of olefins from the dehydration of (bio)alcohols is an important industrial reaction due to the potential for using raw materials from biomass [13–15]. Different catalysts, primarily zeolite ZSM-5 and alumina, have been extensively studied for the conversion of methanol and ethanol to olefins [16–18]. Although Al_2O_3 is considered a standard for use in ethanol dehydration, it adsorbs large amounts of water, leading to decreased activity. This is a significant issue, especially considering that water is present in bioethanol at approximately 10 wt.% [19]. Additionally, deactivation may occur due to coke formation, and more than one product may be produced in the process (e.g., diethyl ether and ethylene). Therefore, there is still a need to develop catalysts for alcohol dehydration that selectively produce hydrocarbons.

Salts of HPW are important alternatives for tuning the strong acidity of this HPA. The substitution of protons with other cations modifies its properties (e.g., acidity, solubility) and can lead to changes in both the secondary structure and activity. For example, Brønsted active sites within the zeolite framework are effectively combined with Lewis centers and additional Brønsted centers by impregnating it with potassium tungstophosphate (K_xHPW), leading to enhanced stability and activity [20].

The higher selectivity of neutral K_3HPW for diethyl ether over ethylene is attributed to Brønsted sites originating from metal cations [21]. These sites, which function as Lewis acids and remain unattached to the support, are more exposed in the composites. Overall, the findings indicate that HPW-supported nanocomposites serve as highly effective and practical solid catalysts for the vapor-phase dehydration of ethanol and the production of ethylene. Additionally, these catalysts are both reusable and environmentally friendly, making them suitable for this crucial industrial process [21].

Based on literature data, it can be inferred that ethylene production is preferred on the acid sites of W-based HPAs, whereas acetaldehyde formation via a dehydrogenation reaction is favored on the basic sites of Mo-based HPAs [22]. Ethanol dehydration and dehydrogenation rates for pure Cs_1HPMo salt and Cs_1HPMo/SBA-15 catalysts were measured as a function of temperature (463–573 K). The inclusion of SBA-15 support significantly enhances ethanol dehydration rates, along with the formation rates of ethylene and acetaldehyde [22].

In addition, it should be noted that catalysts based on supported HPAs are important alternatives for various dehydration and esterification reactions (e.g., glycerol to acrolein, long-chain fatty acids reacting with alcohols to form biodiesel) [23–33]. It has been observed in these studies that the authors tuned the acidity and specific surface area of the catalysts by modifying the loading and the nature of HPW, as well as the nature of the support—specifically, by using mesoporous materials that enhanced catalytic properties. The acidity varied widely, depending on the combination of Brønsted and Lewis sites, which is beneficial for acid-catalyzed reactions that require different acid strengths.

Thus, this work focused on the comprehensive synthesis of silver salt derivatives of HPW (Ag_xPW) using the ion exchange method. The structural and textural properties of these catalysts were fully characterized. The activity of these salts was tested in the model reaction of ethanol dehydration. The most promising catalyst was then supported on SBA-15. The conversion and selectivity to ethylene were discussed in terms of accessibility, acidity, and textural properties of the catalysts.

Experimental

Preparation of $Ag_xH_{(3-x)}PW_{12}O_{40}$ (Ag_xHPW)

To identify the most active AgxHPW salt before its support on SBA-15, all Ag derivatives of HPW ($Ag_xH_{(3-x)}PW_{12}O_{40}$ salts, where x = 1.0, 1.5, 2.0, 2.5, 3.0) were prepared and characterized following the procedure described by Haber et al. [5]. Silver nitrate (99.9%, Sigma-Aldrich, USA) was dried under vacuum at 25 °C for 2 h before solution preparation. The concentration of HPW (99.9%, Sigma-Aldrich, USA) was determined using UV–Vis spectrophotometry (Beckman, model DU 650, USA) with an analytical standard curve of the acid, which had been dried at 200 °C for 4 h prior to analysis. The maximum absorbance readings were at 260 nm, as per the standard HPW solution preparation procedure [34].

The Ag_xHPW salts were obtained by adding volumes corresponding to the desired stoichiometric amounts of $AgNO_3$ solution (0.1 mol L^{-1}) to the HPW solution (0.08 mol L^{-1}) at an approximate rate of 1 mL min^{-1} under constant magnetic stirring. The resulting solutions, along with their precipitates, were left to stand for 12 h, then evaporated at 40 °C until dry. The solids were then calcined at 300 °C for 4 h.

Synthesis of ordered mesoporous silica SBA-15

The mesoporous silica was synthesized following the procedure described by Zhao et al. [8]. For this synthesis, 4 g of the triblock copolymer surfactant Pluronic P123 (PEO20-PPO70-PEO20—poly(ethylene oxide)-poly(propylene oxide)-poly(ethylene oxide), Aldrich, USA) was dissolved in 100 mL of 1.6 mol L^{-1} HCl (37%, Vetec, Brazil). The solution was mixed and heated to a constant

temperature of 35 °C using a heating/magnetic stirring plate. After complete dissolution, 7.5 mL of the silica precursor tetraethylorthosilicate (TEOS, 98%, Sigma-Aldrich, USA) was added under stirring. The mixture was then distributed into autoclaves, which were heated to 100 °C for 48 h. The resulting product was filtered and dried at 50 °C. The dried material was calcined in a tubular furnace in two stages: first, at 300 °C for 4 h under nitrogen flow, and then at 540 °C for 8 h under atmospheric air flow, with a heating rate of 2 °C min⁻1.

Preparation of the supported catalyst (20%Ag_2HPW/SBA-15)

The 20 wt.% Ag_2HPW/SBA-15 composite was prepared following an adapted procedure by Holclajtner-Antunovic et al. [35], using appropriate amounts of precursors to synthesize Ag_2HPW. Silver nitrate was dissolved in a methanol–water mixture (1:1) and supported on SBA-15 by incipient impregnation. The sample was aged for 24 h, dried at 110 °C, and then calcined at 300 °C for 3 h. Subsequently, HPW was impregnated using an aqueous solution, followed by the same aging, drying, and calcination steps described for $AgNO_3$.

Analytical techniques for characterization

Powder diffraction patterns of the materials were obtained using a Bruker D8 Focus diffractometer (θ–2θ, Germany) with CuKα radiation (λ = 0.15418 nm), operated at a tube power of 40 kV and 30 mA. The 2θ diffraction angle was scanned in the range of 2° to 60° at an angular velocity of 1° min⁻1.

Fourier transform infrared spectroscopy (FT-IR) was conducted over the 4000–400 cm^{-1} region using a Thermo Scientific Nicolet 6700 spectrometer (USA) equipped with a mercury-cadmium-telluride (MCT) detector maintained at liquid N_2 temperature (77 K). Measurements were performed using KBr pellets, resolution of 4 cm^{-1} and 128 scans.

Small-Angle X-Ray Scattering (SAXS) experiments were conducted using a Bruker Nanostar setup (Germany) equipped with a two-dimensional filament detector and a vacuum chamber. The experimental parameters were as follows: X-ray wavelength λ = 0.15418 nm, power output of 1.5 kW, collimation provided by a Gobel mirror system and three slits, q range of 0.13 to 3.4 nm⁻1, and a 20-min exposure time for data collection.

The thermal stability of the catalysts was verified using TG/DTG curves obtained with a TA-Instruments SDT 2960 thermal analyzer (USA). The measurements were performed under a flow of 110 mL min^{-1} of synthetic air (99.999%) at a heating rate of 10 °C min^{-1} over a temperature range of 25–700 °C.

The specific surface area, pore diameter, and pore volume of the solids were determined using a gas sorption system obtained with a Micromeritics ASAP 2020C (USA) under nitrogen gas at −196 °C during the adsorption and desorption processes. The specific surface area was calculated based on the Brunauer-Emmet-Teller

(BET) adsorption isotherm, the total pore volume (V_p) was measured at $P/P_0 = 0.98$, and the average pore diameter was determined using the Barrett-Joyner-Halenda (BJH) model. The samples (approximately 0.5 g) were pretreated at 300 °C for 6 h under vacuum to remove water and degasify the solids.

Scanning Electron Microscopy (SEM) images were obtained using a field emission scanning electron microscope from Jeol JSM-7001S (Japan) operating at 15 kV. The powdered sample was fixed onto a double-sided carbon tape on the stub and metallized with platinum.

Solid-state nuclear magnetic resonance (MAS NMR) spectra were obtained in a spectrometer using a Bruker Avance III HD Ascend (Germany) of 14.1 T (600 MHz relative to the ^{1}H nucleus). A 4 mm CP/MAS solid probe was used, and the samples were packed into a zirconia rotor with the following specific conditions for each nucleus: ^{29}Si (119.3 MHz) at a rate of 10 kHz, pulse duration of 4.25 µs (90° flip angle), interval between pulses of 20 s and minimum of 1024 acquisitions. The reference used was $Si(CH_3)_4$ (TMS, $\delta = 0$ ppm); ^{31}P (243.1 MHz) at a rate of 10 kHz, pulse duration of 4.75 µs (90° flip angle), pulse interval of 10 s and 64 acquisitions. The reference used was $NH_4H_2PO_4$ ($\delta = 0.9$ ppm relative to H_3PO_4, $\delta = 0$ ppm). The ^{31}P spectra were referenced to H_3PO_4, making the necessary displacement.

Ethanol dehydration reaction

The ethanol dehydration reaction run in a pulse microreactor coupled to a gas chromatography system (Shimadzu, model GC-FID 2010, Japan) using a column Shimadzu CBP1 PONA-M50-042 (50.0 m × 0.15 mm × 0.33 µm) [13]. For each analysis, 0.1 µL of ethanol (99%, Vetec, Brazil) was injected into the reactor (liner) containing 10 mg of the catalyst. The catalyst was in the form of pellets (355 to 710 µm) and was activated at 300 °C for 1 h before reaction. The GC programming conditions were: pressure of 146.1 kPa; total flow of 231 mL min^{-1}; column flow of 2.24 mL min^{-1}; linear velocity of 44 cm s^{-1}; purge flow of 5 mL min^{-1}; split ratio of 100; temperature of the column at 40 °C for 1.5 min and then ramped to 70 °C; Helium carrier gas; flame detector (FID) temperature of 250 °C; injector temperature of 200 to 400 °C. The approximate weight hourly space velocity (WHSV) was 11.3 h^{-1}. A sequence of 5 injections of ethanol was performed, generating a chromatogram whose peaks were integrated to calculate the conversion and selectivity. The results were reported as average. The error on the calculated conversions was about 2%. The calculation for conversion of ethanol, selectivity for ethylene (EE) and diethyl ether (DEE) were defined by Eqs. (1) to (3), where n is the number of moles:

$$\text{Conversion}\ (\%) = \frac{n_{\text{ethanol initial}} - n_{\text{ethanol final}}}{n_{\text{ethanol initial}}} \times 100 \tag{1}$$

$$\text{Selectivity}\ (\%) = \frac{n_{\text{EE}}}{n_{\text{ethanol initial}} - n_{\text{ethanol final}}} \times 100 \tag{2}$$

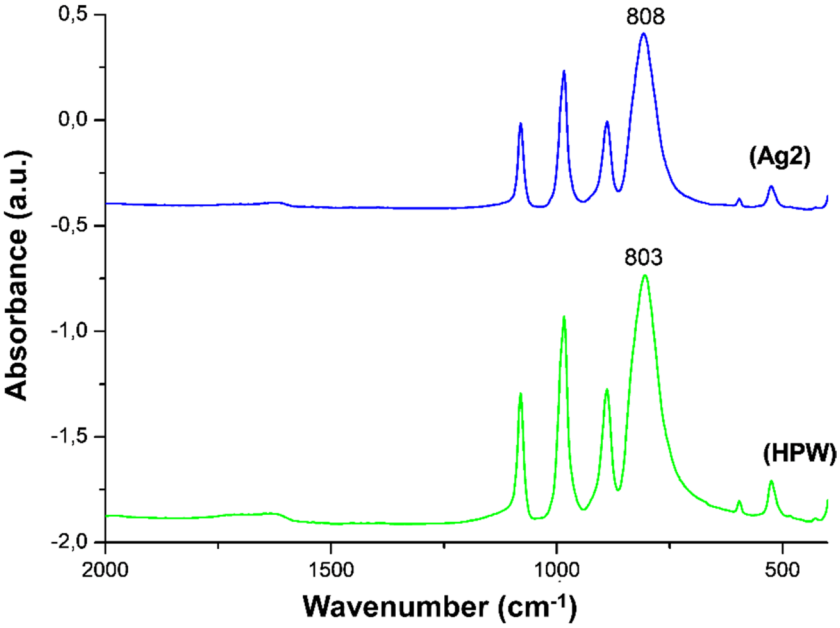

Fig. 1 FT-IR spectra of HPW and Ag_2HPW, both calcined at 300 °C

$$\text{Selectivity } (\%) = \frac{n_{DEE}}{n_{ethanol\,initial} - n_{ethanol\,final}} \times 100 \tag{3}$$

Results and discussion

Characterization of Ag_xHPW

The silver salts of HPW were characterized by means of various techniques (EDXRF, FT-IR, XRD, ^{31}P MAS NMR and TG/DTG). The data confirmed the composition, structure, and thermal stability of each salt in the synthesized series. The Keggin structure was confirmed by the fingerprint bands in the FT-IR spectra as well as ^{31}P MAS NMR, which agreed with literature reports [6, 35]. The complete characterization data are available in the Supplementary Information. As the most important salt in our application was Ag_2HPW (see justification in Sect. "Ethanol dehydration model reaction"), this catalyst was described in detail.

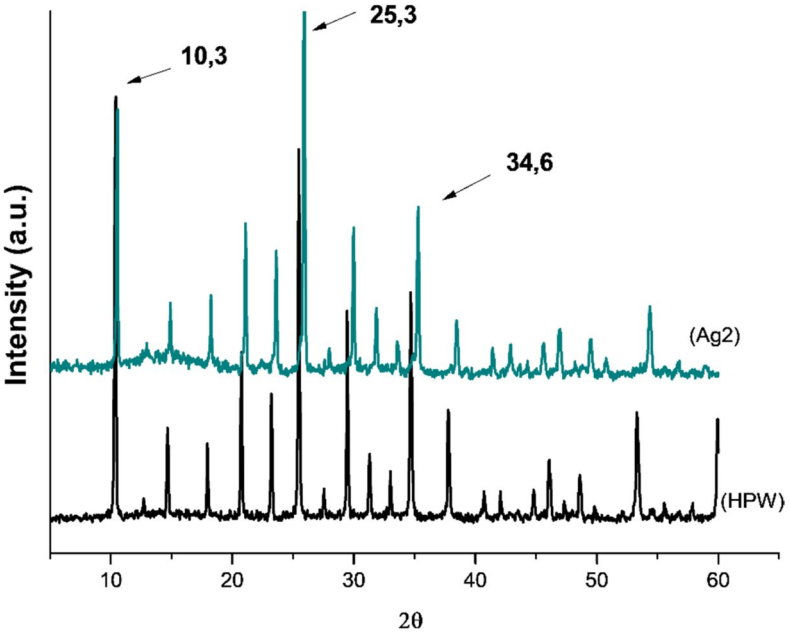

Fig. 2 Powder XRD of HPW and Ag_2HPW, both calcined at 300 °C

Characterization of $Ag_2HPW_{12}O_{40}$ (Ag_2HPW)

FT-IR spectroscopy

The primary structure of the Ag_2HPW salt was investigated using infrared spectroscopy. Figure 1 shows the FT-IR spectra of the synthesized Ag_2HPW salt and HPW in the Keggin anion fingerprint region. The vibrational bands characteristic of HPW were located at 1080, 983, 887, and 803 cm^{-1} [36, 37], corresponding to ν_{as} (P-O_a) of the central phosphorus atom, terminal ν_{as} (W = O_t), corner-sharing ν_{as} (W-O_c-W), and edge-sharing ν_{as} (W-O_e-W), respectively, related to the different oxygen atoms in the Keggin structure. There was only a slight shift in the vibration band of ν_{as} W-O_e-W (803 to 808 cm^{-1}), which is related to both the hydration degree and the counter cation of the Keggin anion [2, 6, 37]. Thus, the absorption band positions for Ag^+ salts indicated that the Keggin anion structure was maintained in all salt derivatives when protons were partially or totally replaced by the silver cations, as observed in the literature [38].

Powder XRD and SEM analysis

Another investigation of the structure of the Ag_2HPW salt was conducted using X-ray diffraction. This method provided information about the secondary structure. Pure HPW exhibits characteristic diffraction peaks at 2θ = 10.3°, 25.3°, and 34.6° (Fig. 2) and has a unit cell parameter of 1.21 nm [39]. The exchange of the

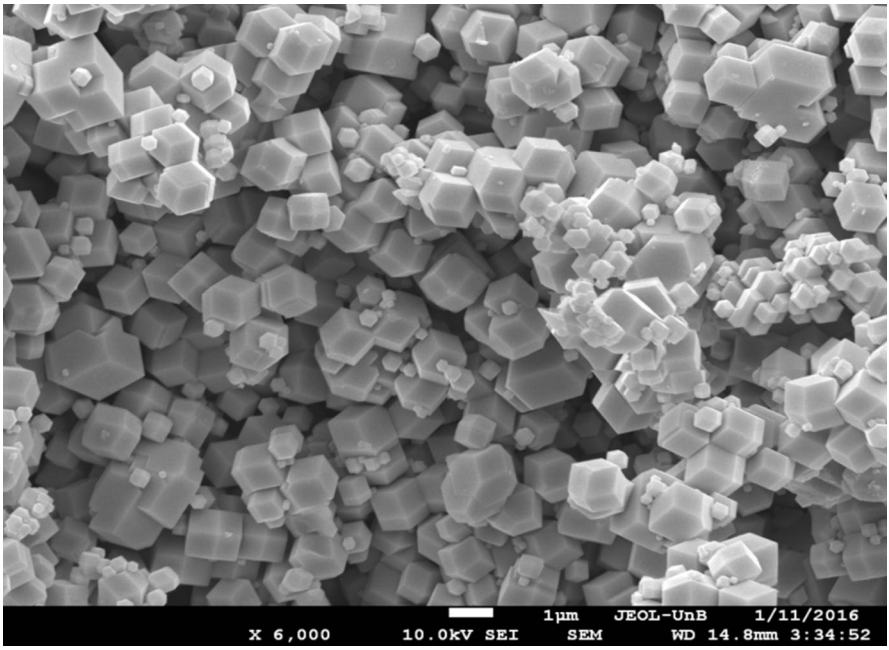

Fig. 3 SEM image of Ag_2HPW calcined at 300 °C

acid protons in its secondary structure, in the form of $H_5O_2^+$ (hydronium ions), with hydrated silver cations results in the contraction of the unit cell [5, 40]. This behavior, involving a decrease in the cell parameter, has been observed for other monovalent salts (K^+, NH_4^+, Cs^+, Ag^+, and Rb^+) of HPW and has been described in the literature [5, 39, 40]. Each diffraction pattern indicated the existence of a single crystalline phase, with reflections closely resembling those of the cubic structure of $H_3PW_{12}O_{40}{\cdot}6H_2O$, suggesting that the silver salt derivatives are derived from the Keggin HPW structure. Therefore, the prepared salt retained the original Keggin structure after the partial ion exchange of acidic protons with silver cations, as confirmed by both FT-IR and X-ray diffraction.

The crystallite size domain of the silver salt was calculated using the Scherrer equation [41]. For this analysis, the angle at $2\theta = 25.3°$ (hkl 110) was used as the most significant (highest intensity). The average size of the crystallite domain for the Ag_2HPW salt was about 63 nm, which agreed with the literature [42]. The morphological grain sizes of the silver salts are on micrometer scale (i.e., dodecahedron and cubic shapes, according to the SEM image in Fig. 3). This can be explained by a supposed aggregation mechanism, where the epitaxial interfaces are formed to give a thermodynamically stable morphology. Many epitaxial nanocrystals are attached to each other, thus making their crystalline planes coherent. The epitaxial interfaces of the silver salts are formed by the slight dissolution and reprecipitation of the nanocrystals [5].

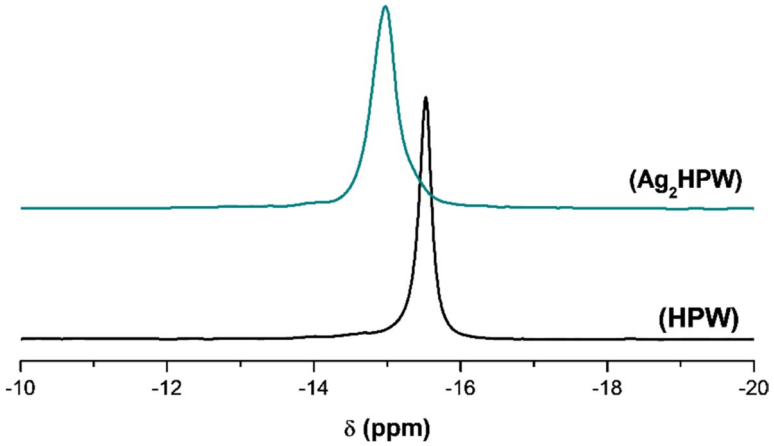

Fig. 4 ^{31}P MAS NMR spectra of hydrated HPW and Ag_2HPW

^{31}P MAS NMR spectroscopy

The exchange of protons with silver atoms causes a small increase in the electronic density of the phosphorus nucleus, resulting in the displacement of the magnetic field of the central phosphorus atom in the Keggin structure. This is demonstrated by the ^{31}P MAS NMR spectra of the solid silver salts, which depend on the degree of hydration [43]. In HPW·nH_2O, δ values range from −15.9 to −14.7 ppm for n = 6 and −11.1 to −10.5 ppm for n = 0, respectively, according to the literature [43, 44]. In HPW·6H_2O, the acid protons are bound to the water of crystallization, forming hydronium ions ($H_5O_2^+$) that connect to the polyanion through the terminal oxygen via hydrogen bonding. In the anhydrous acid, the protons are bound directly to the terminal oxygen atoms of the polyanion. Therefore, the samples present a single signal in the spectra, which shifts in the field from −15.5 to −14.9 ppm in HPW and Ag_2HPW, respectively (Fig. 4). The single signal in the salt is related to the homogeneous distribution of species (H^+ and Ag^+) around the phosphorus atom, creating similar chemical environments. As the displacement is close to that of hydrated HPW (−15.5 ppm), we can conclude that in this salt, the protons are not directly bound to the polyanions but are forming $H_5O_2^+$ ions that bind to the terminal oxygen [40].

Acidity of Ag_xHPW salts

FT-IR was used to determine the type of acid sites on each catalyst by adsorbing a probe molecule, such as pyridine. The concentration of Brønsted (pyridinium ion formation), Lewis, and hydrogen bond sites can be determined by the interaction of the pyridine molecule with the acidic solids [45, 46]. The FT-IR spectra of adsorbed pyridine showed the presence of pyridine vibration bands at 1635, 1612, 1540, and 1487 cm^{-1} for all silver salts, except for Ag_3PW, which exhibited a large band at 1620 cm^{-1} (Fig. 5). The band appearing at 1428 cm^{-1}

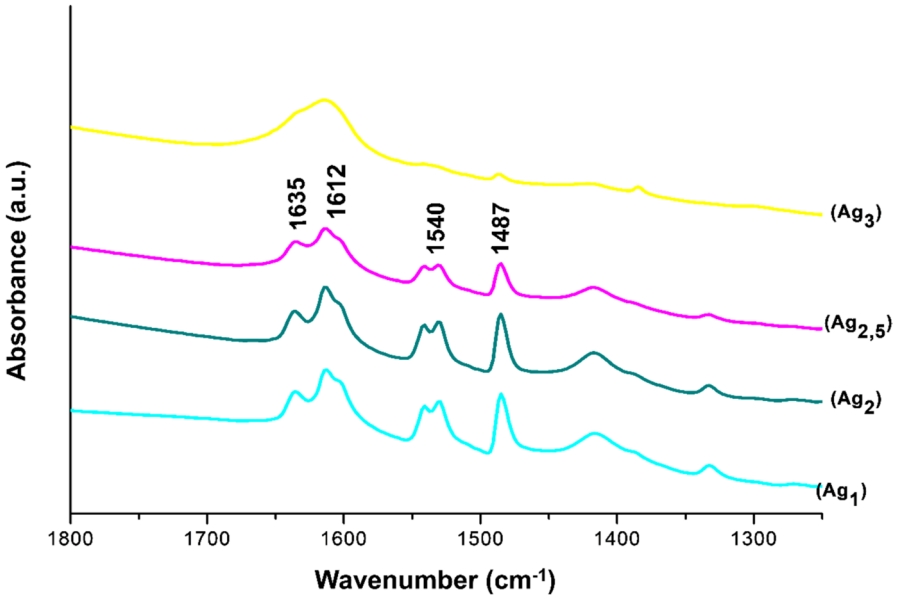

Fig. 5 FT-IR spectra of pyridine adsorbed on Ag_xHPW salts

may correspond to either a Lewis band or physically adsorbed pyridine [45]. The band at 1487 cm^{-1} is a combination of Brønsted and Lewis acid sites, while the bands at 1540 and 1612 cm^{-1} are associated with the formation of pyridinium ions (i.e., adsorption of pyridine onto Brønsted sites) on the catalysts. The presence of the shoulder observed at 1540 cm^{-1} is related to the formation of pyridinium ions interacting with another pyridine molecule. This could occur because the experimental adsorption system, which operates under N_2 flow rather than a vacuum regime, might not allow the complete desorption of physically adsorbed pyridine. The band at 1635 cm^{-1} is attributed to hydration water in the material. Bands related to pyridinium ion formation and hydrogen bonding are associated with acidic centers containing O–H bonds, with little or no evidence of Lewis acid sites [7]. The acidic properties of the pure heteropoly salts arise from the presence of residual protons derived from the HPW and/or water molecules coordinated to the silver cation, which were introduced into the heteropoly salts. Thus, it can be concluded that both Brønsted and Lewis sites are present on the silver HPW salts.

Characterization of ordered mesoporous silica SBA-15

The successful synthesis of SBA-15 can be determined by various methods that are used in the literature, such as SAXS, FT-IR, ^{29}Si MAS NMR, SEM, TEM, and textural analysis by N_2 adsorption. The detailed characterization of our synthesized SBA-15 is provided in the Supplementary Information (SI).

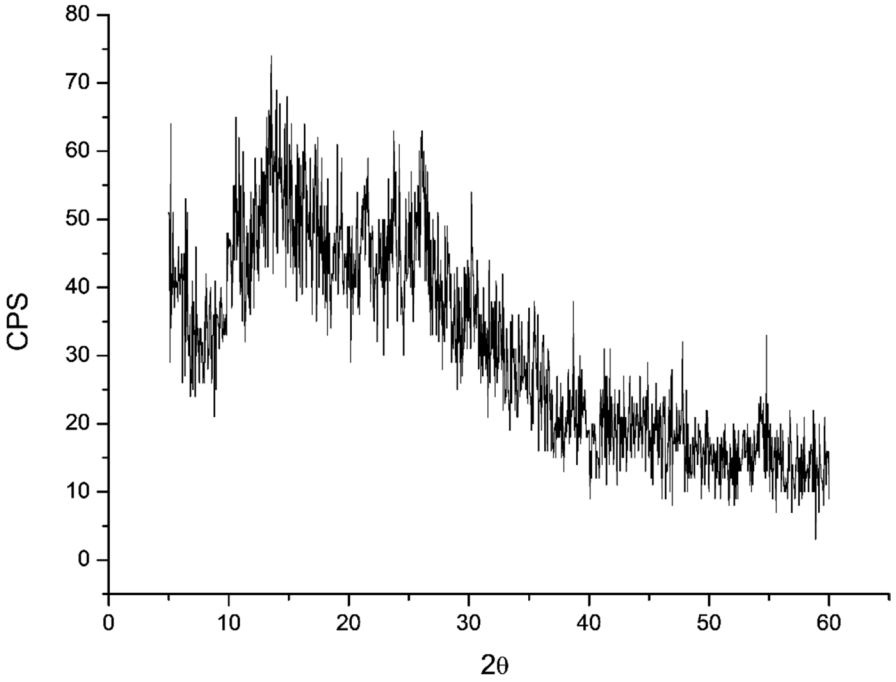

Fig. 6 XRD of 20%Ag_2HPW/SBA-15 calcined at 300 °C (in counts per second, CPS)

Characterization of the 20%Ag_2HPW/SBA-15 catalyst

Elemental, XRD and SAXS analysis

The elemental analysis of the supported Ag_2HPW showed that the actual loading was 19.8 wt.% of the salt. Because of the similar values, the nominal one is maintained throughout the manuscript.

The XRD pattern of the 20% Ag_2HPW/SBA-15 composite is shown in Fig. 6. Although SBA-15 can accommodate many active phases due to its large pore volume and high specific surface area, no typical HPW crystalline phase diffraction peaks are observed in the XRD. This absence indicates that Ag_2HPW particles are likely highly dispersed on SBA-15 [35]. This is further corroborated by the calculation of monolayer formation on SBA-15, as it has a very high BET specific surface area (650 $m^2\ g^{-1}$) and a 20 wt.% loading that is far from saturation (the coverage is only 0.08) [46].

The structure of the SBA-15 was examined by Small-Angle X-ray Scattering (SAXS). Five peaks were clearly observed in the curves (Fig. 7), indexed according to the bi-dimensional hexagonal symmetry of the pore arrangement (*p6mm*). The curves were obtained for the pristine sample, heat-treated at 300 °C (TT300), and supported Ag_2HPW on SBA-15. The SAXS data were fitted using the model reported in the literature [47]. The most important parameters are listed in Table 1. The very small decrease in the lattice parameter after thermal treatment was

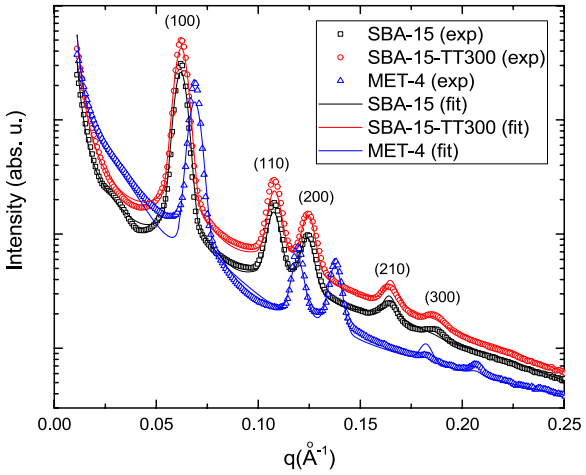

Fig. 7 SAXS curves of SBA-15 (∀), SBA-15 calcined at 300 °C for 3 h, TT300, (–), 20%Ag_2HPW/SBA-15, MET-4, (Δ) and the respective fitting results (line)

Table 1 Lattice parameter (a_0), pore diameter (D) and pore electronic density ratio ($\Delta\rho_{out}/\Delta\rho_{in}$)

Catalyst	a_0 (nm)	D (nm)	$\Delta\rho_{out}/\Delta\rho_{in}$
SBA-15	11.7	10.8	5.2
SBA-15—TT300	11.6	10.2	8.2
20%Ag_2HPW/SBA-15	10.5	9.0	2.9

expected due to densification of the walls, which caused shrinkage of the structure. This decrease became more pronounced after the incorporation process of Ag_2HPW, due to an additional heat treatment at 110 °C, in addition to the heat treatment at 300 °C. The increase in the electronic density contrast ($\Delta\rho_{out}/\Delta\rho_{in}$) ratio between samples of SBA-15 (pristine and TT300) was attributed to densification of the silica walls after the heat treatment, leading to an increase in $\Delta\rho_{out}$. On the other hand, the presence of the Ag_2HPW salt inside the mesopores decreased this electronic density contrast ratio due to an increase in $\Delta\rho_{in}$. The fitting results agreed with the experimental curves, but it is important to note that the 20% Ag_2HPW/SBA-15 sample exhibited additional scattering at low (q), which can be attributed to the presence of catalytic particles outside the OMS, on top of the silica cylinders. This may partially block the entrance to the mesopores in SBA-15.

^{31}P MAS NMR spectroscopy

The ^{31}P MAS NMR spectrum can detect the Keggin unit on the supported catalyst (Fig. 8). The sample showed only a characteristic signal at −15.2 ppm of Ag_2HPW after the impregnation and calcination processes, which confirmed the maintenance of the Keggin structure, as already discussed for Ag_xHPW salts in the SI section [43].

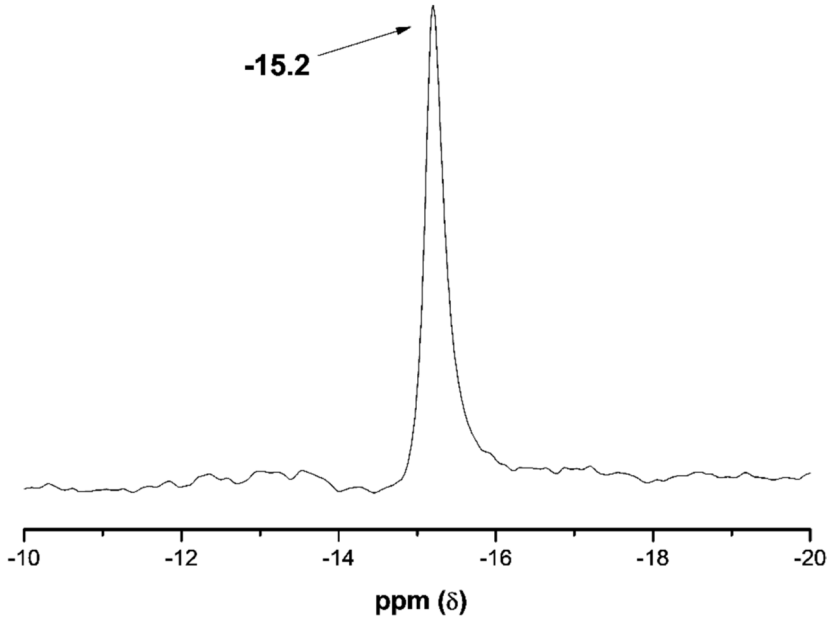

Fig. 8 ^{31}P MAS NMR of 20%Ag_2HPW/SBA-15 calcined at 300 °C

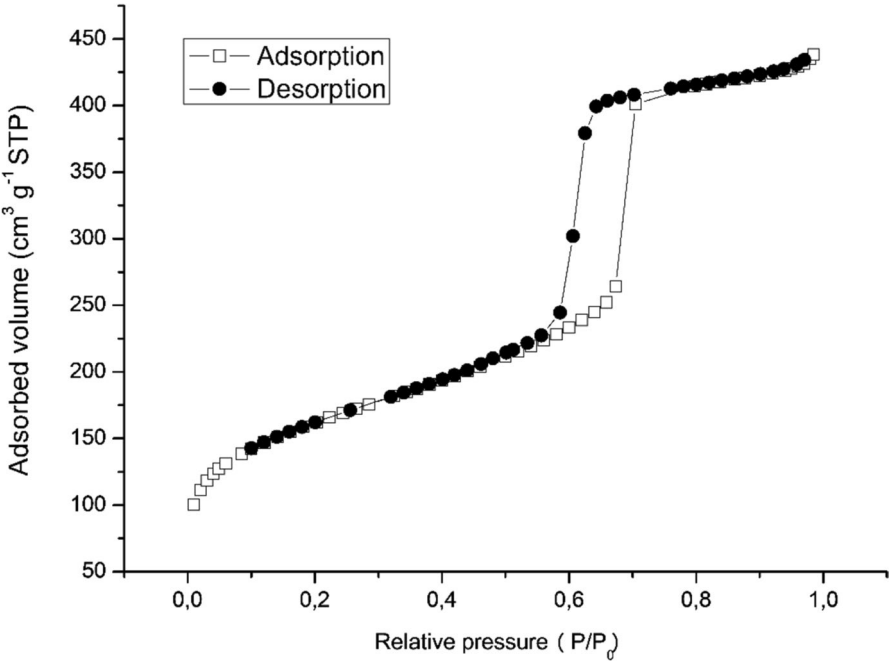

Fig. 9 N_2 isotherm of adsorption/desorption on 20%Ag_2HPW/SBA-15 catalyst

Table 2 Main textural properties of the catalysts

Catalyst	S_{BET} (m^2/g)	D_p (nm)	V_p (cm^3/g)
Ag_2HPW	5	3.1	0.01
SBA-15	687	6.1	1.10
20%Ag_2HPW/SBA-15	576	6.0	0.89

N_2 adsorption/desorption isotherms at −196 °C

The 20% Ag_2HPW/SBA-15 catalyst also showed an N_2 adsorption/desorption isotherm of type IV(a) and hysteresis type H1 (Fig. 9), as defined by IUPAC [48], which are characteristic of mesoporous materials [8–10]. The textural properties of the composite were determined from the isotherm using different models, summarized in Table 2, which identify the changes in these parameters after the deposition of Ag_2HPW on SBA-15. After impregnation of 20% Ag_2HPW on SBA-15, the specific area of the active phase increased, whereas the BET specific surface area of SBA-15 decreased by about 17%. This is consistent with the SAXS measurements, which demonstrated that the incorporation of Ag_2HPW nanoparticles onto the SBA-15 surface led to partial blocking of the SBA-15 mesopores. Therefore, the pore volume and the average pore diameter underwent a slight decrease.

SEM analysis

Figure 10a–b shows SEM micrographs (10 µm different scales) of the composite 20%Ag_2HPW/SBA-15, calcined at 300 °C. After Ag_2HPW impregnation, the images show needle-like shapes, suggesting that the impregnation process did not change the morphology of the original SBA-15 sample (as described in the SI section). Clusters in the material were observed when Ag_2HPW was impregnated on the surface structure, as also observed for pure HPW [49]. The apparent fibrous crystals on the surface might be the result of acidic reaction on the silica surface during the impregnation of HPW, which is known to be a very strong acid in solution [2]. In addition, deposition of Fe_3O_4 on the SBA-15 surface also showed similar images to the Ag_2HPW impregnation [50]. It may be concluded that the presence of 20% Ag_2HPW on SBA-15 did not significantly affect the morphology of the mesoporous material.

Ethanol dehydration model reaction

Firstly, the pure salts of AgxHPW were tested in the dehydration of ethanol to evaluate their relative activities in ethylene production. The results are shown in Table 3, along with the specific surface area of these salts. It can be observed that the ethanol conversion was below 30%, despite the high selectivity to ethylene (≥93%). It is important to note that the error in these calculations was approximately 2%, based on an average of at least five pulsed experiments. Ethanol conversion is linked to the

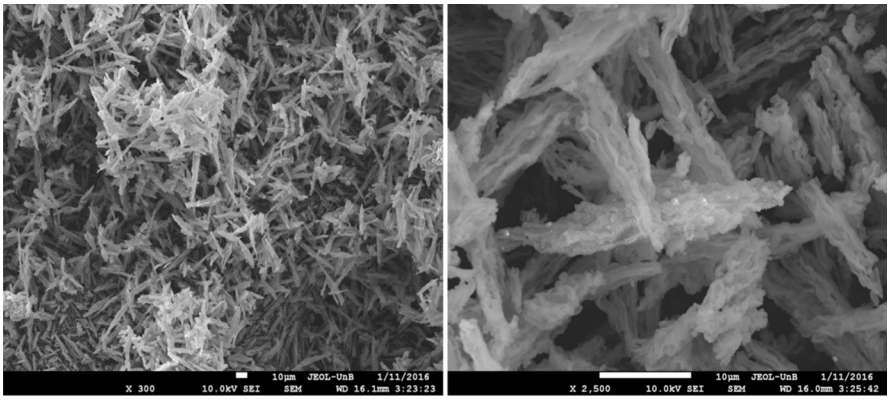

Fig. 10 SEM image of 20%Ag_2HPW/SBA-15 calcined at 300 °C

Table 3 Conversion (C) and selectivity (Sel) to ethylene (EE) and diethyl ether (DEE) for ethanol dehydration at 200 °C using the Ag_xHPW catalysts (x = 1; 2; 2.5 and 3) activated at 200 °C

Ag_xHPW	S_{BET} (m^2/g)	C (%)	Sel EE (%)	Sel DEE (%)
Ag_1HPW	2.9	20.4	93.2	6.8
Ag_2HPW	4.8	27.8	97.5	2.5
$Ag_{2.5}$HPW	4.0	13.2	96.0	4.0
Ag_3HPW	4.7	4.1	94.9	5.1

presence of protons from HPW, as well as those generated from water coordinated with silver cations, as shown in Eq. 4:

$$Ag^+ + mH_2O \rightarrow \left[Ag\left(H_2O\right)_m\right]^+ \rightarrow \left[Ag\left(H_2O\right)_{m-1}(OH)\right]^{(m-1)+} + H^+. \quad (4)$$

Accordingly, the ethanol conversion is clearly dependent on the acidity of the catalysts. The higher the amount of Ag^+ cations substituted in HPW, the lower the proton acidity of the catalysts, as already established in the literature [5]. Table 3 displays the same trend for ethanol conversion, except for Ag_1HPW, which had a lower conversion than Ag_2HPW. The higher activity of Ag_2HPW in the series can be attributed to its slightly higher specific surface area, although all the areas are very low, i.e., in the same order of magnitude as that of HPW (~ 5 m^2 g^{-1}). In neutral Ag_3HPW, only residual protons can be present in the salt, which may explain the very low activity. It is known from the literature [7, 51, 52] that the absence of protons, which generate Brønsted acidity, can be overcome by pretreating the solid with water vapor, thus producing a bifunctional catalyst when the reaction cannot provide sufficient moisture to form these acid sites. Because our ethanol was about 99%, some water was provided, which might have contributed some extra catalytic activity for this salt. Matachowski et al. [52] showed that reaction temperatures above 250 °C cause the loss of water molecules coordinated to silver cations and, consequently, the tertiary structure of Ag_xHPW salts is also affected, forming pores with smaller diameters due to the closer approximation of the Keggin ions. As a result,

Table 4 Effect of the temperature on the activity of Ag_2HPW catalyst (activated at 300 °C) in ethanol conversion (C) and selectivity for ethylene (EE) and diethyl ether (DEE)

Temperature (°C)	C (%)	Sel EE (%)	Sel DEE (%)
400	77.1	99.4	0.6
350	69.9	99.2	0.8
300	63.5	95.2	4.8
250	50.2	91.5	8.5
200	25.8	72.6	27.4

Table 5 Conversion (C) and selectivity (Sel) to ethylene (EE) and diethyl ether (DEE) of the ethanol dehydration reaction with 20%Ag_2HPW/SBA-15 and pure Ag_2HPW (both activated at 300 °C) at different temperatures (T)

Catalyst	T (°C)	S_{BET} (m^2/g)	C (%)	Sel EE (%)	Sel DEE (%)
Ag_2HPW	300	4.7	63	95	5
20%Ag_2HPW/SBA-15	300	576	86	88	12
Ag_2HPW	400	4.7	77	98	2
20%Ag_2HPW/SBA-15	400	576	100	100	0

this directly interferes with the catalytic activity of heteropoly salts. Thus, the low conversion can be attributed to the low number of protons accessible on the surface, i.e., most protons are located in the bulk structure of the salts. Additionally, the similarity in ethylene selectivity is likely because the strength of the surface protons is sufficient to convert ethanol into this product.

Therefore, considering the highest conversion and selectivity to ethylene in the series, the best catalyst was the Ag_2HPW salt, which was further studied for the same reaction at different temperatures (Table 4). It was observed that both conversion and selectivity to ethylene increased with temperature. This increase in activity (conversion) and selectivity was already expected based on thermodynamic and kinetic principles. Literature studies [5, 53] have shown that, in acidic ethanol dehydration, diethyl ether is the main product at lower temperatures (below 180 °C), whereas ethylene formation predominates at higher temperatures. Additionally, different activation conditions for Ag_2HPW (200 °C vs. 300 °C, Tables 3 and 4) demonstrated that water plays an important role in the product selectivity of Ag_xHPW. When comparing the dehydration reactions at the same temperature (200 °C), the lower conversion and selectivity to ethylene at the higher activation temperature (300 °C) suggested a decrease in acidity in the Ag_2HPW salt. This can be explained by the known dehydration mechanism, which relies on proton accessibility [14], a factor that is reduced due to shrinkage of the cell parameter [44, 52–56]. Moreover, the very low specific surface area of Ag_2HPW may prevent ethanol from reaching all the protons on the solid during surface-type reactions. In this context, Ag_2HPW was chosen to be supported on SBA-15, allowing its nanocrystals to be exposed on the high surface area of the mesoporous silica, thereby improving accessibility to the active sites. A 20 wt.% loading was selected because previous studies have shown

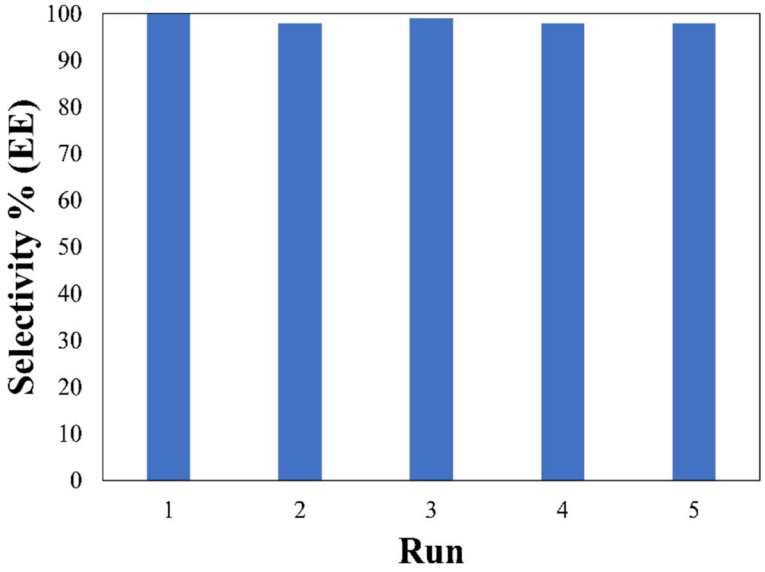

Fig. 11 Catalyst (20%Ag_2HPW/SBA-15) reutilization in five consecutive ethanol dehydration reactions at 400 °C

good activity for 20–30% loading systems [5, 24, 35]. Furthermore, this loading is less than 10% of the monolayer coverage for this supported catalyst.

The effect of supporting Ag_2HPW on SBA-15 was studied at temperatures of 300 and 400 °C (Table 5). The catalysts (pure Ag_2HPW and 20%Ag_2HPW/SBA-15) were pre-activated at 300 °C before the reaction. Activation of the supported Ag_2HPW at 300 °C is crucial to enhance hydrogen bonding interactions with SBA-15, forming a more stable composite. The parent SBA-15 was not active for ethanol dehydration under the same experimental conditions, as previously reported [11]. A significant improvement in ethanol conversion and selectivity to ethylene was observed when using the 20%Ag_2HPW/SBA-15 catalyst. The acidity of SBA-15 is very low compared to Ag_2HPW, as measured by calorimetry [11]. Furthermore, the number of protons (Brønsted sites) is much lower (0.20 mmol g^{-1} for 20%Ag_2HPW/SBA-15 versus 0.32 mmol g^{-1} for Ag_2HPW). Thus, the improvement in conversion can primarily be attributed to the increase in specific surface area. The incorporation of the active phase (Ag_2HPW) onto the mesoporous surface support greatly enhanced accessibility to the Brønsted sites. The high dispersion of Ag_2HPW on SBA-15, confirmed by the absence of a crystalline phase in the XRD analysis, indicates the presence of nanocrystals of Ag_2HPW on the SBA-15 surface, which facilitates better access to the protons in their secondary structure. Haber et al. [5] studied the $Ag_xH_{(3-x)}PW_{12}O_{40}$ and $K_xH_{(3-x)}PW_{12}O_{40}$ (x = 1–3) salts supported on SiO_2, which were used in ethanol dehydration reactions in a continuous flow reactor. Their results showed a decrease in ethanol dehydration activity with increasing silver content (x) at temperatures below 300 °C. However, at 400 °C, all salts exhibited similar activity levels. Therefore, our results suggest that the investigated salt (Ag_2HPW) is

a promising catalyst for ethylene production, but its support on mesoporous matrices significantly enhances its performance. Moreover, the 20%Ag_2HPW/SBA-15 catalyst is more cost-effective due to the use of a diluted active phase.

The reutilization of the 20%Ag_2HPW/SBA-15 catalyst was tested in five consecutive injections of ethanol at 400 °C. The conversion remained approximately constant (98–100%), and the selectivity to ethylene is shown in Fig. 11. It was observed that the catalyst maintained its original performance; however, no further structural analysis was conducted.

The literature [57–62] has explained the process of ethanol conversion through four main types of reactions: dehydration, dehydrogenation, dehydrogenation coupling, and hydrogenolysis. In each case, aside from the pure thermal process, the reaction is primarily governed by the active sites present in the catalysts. Specifically, dehydration occurs via an intramolecular mechanism in which the oxygen (from the hydroxyl group) attacks the labile hydrogen of the acid catalyst, leading to water release. The resulting primary carbocation is then attacked by the conjugate base of the catalyst, regenerating it, and forming ethylene as the product. A concurrent intermolecular dehydration reaction can also occur, producing diethyl ether (DEE), which undergoes further dehydration. Additionally, ethylene may undergo subsequent reactions, leading to a variety of possible products (e.g., oligomerization, cracking). The key factor determining selectivity for a particular product is the nature of the active sites. When using solid acid catalysts, controlling the number and strength of Brønsted sites is critical for enhancing selectivity. In this regard, our 20%Ag_2HPW/SBA-15 catalyst performed very well in terms of controlling both the strength and number of acid sites. However, a lingering drawback continues to drive further investigations into new catalysts and catalytic conditions for this dehydration reaction.

Conclusions

This work focused on the systematic synthesis of silver salt derivatives of HPW using the ion exchange method. The salts $Ag_xH_{(3-x)}PW$ (x = 1, 2, 2.5, 3) maintained the original Keggin structure after the total or partial exchange of protons for silver cations, as confirmed by various techniques. FT-IR analysis in the pyridine adsorption range (1400 to 1700 cm^{-1}) revealed the presence of both Brønsted and Lewis sites on all silver HPW salts, except for Ag_3HPW, which predominantly exhibited only Lewis sites. These silver salts had a very low specific surface area (< 5 m^2 g^{-1}). To evaluate the acidity of these catalysts, they were tested in the model reaction of ethanol dehydration at 200 °C. Under these conditions, Ag_2HPW showed the highest ethanol conversion (~ 30%) with high selectivity to ethylene (~ 97%). To further improve conversion, this catalyst was tested at reaction temperatures ranging from 200 to 400 °C and under different activation conditions (200 and 300 °C). Ethanol conversion was found to be dependent on the activation temperature of Ag_2HPW, with hydration degree playing an important role. The lower conversion and selectivity to ethylene at the higher

activation temperature (300 °C) suggested a decrease in acidity of the Ag_2HPW salts due to dehydration; that is, proton accessibility for ethanol was reduced as a result of shrinkage in the cell parameter. To improve this accessibility, Ag_2HPW was supported on SBA-15. The 20%Ag_2HPW/SBA-15 catalyst was highly stable, and the support effectively dispersed the Ag_2HPW nanocrystals on its surface with minimal morphological changes at low coverage (8%). Gas-phase dehydration conditions were optimized to achieve complete conversion, with ethanol fully converted to ethylene at 400 °C. No significant deactivation of the catalyst was observed after 5 pulsed reactions, but no structural parameters of the catalyst were evaluated. Thus, 20%Ag_2HPW/SBA-15 is an option solid acid catalyst for this reaction.

Supplementary Information The online version contains supplementary material available at https://doi.org/10.1007/s11164-024-05481-5.

Acknowledgements We acknowledge Conselho Nacional de Desenvolvimento Científico e Tecnológico, CNPq (Grant numbers 307413/2021-7, 308693/2022-1) and Coordenação de Aperfeiçoamento de Pessoal de Nível Superior, CAPES (Grant Number 001) for research and graduate student scholarships. In addition, we valued the financial support provided by Decanato de Pesquisa e Inovação, Instituto de Química/Universidade de Brasília, DPI/IQ/UnB, Ministério da Ciência Tecnologia e Inovações/Conselho Nacional de Desenvolvimento Científico e Tecnológico, Fundação de Apoio à Pesquisa do Distrito Federal, FAPDF (Grant Numbers 00193-00001144/2021-60 and 00193-000001176/2021-65), Fundação de Empreendimentos Científicos e Tecnológicos, FINATEC, Financiadora de Estudos e Projetos, FINEP/CTPetro/CTInfra, and Petrobras. We are also grateful due to finance by Fundação de Amparo à Pesquisa do estado de São Paulo, FAPESP (Process 08/52084-5). Contribution from Laboratório de Catálise Instituto de Química Universidade de Brasília, Brasília, DF 70910–900, Brazil. http://www.labcat.unb.br.

Author contributions M. R. A. conceptualization, methodology, formal analysis, investigations, data curation, writing. M. C. H. C. methodology, formal analysis, investigations, data curation, review and editing. G. A. V. M. conceptualization, formal analysis, investigations, data curation, writing, review and editing. L. C. C. S. methodology, formal analysis, investigations, data curation, review and editing. M. C. A. F. methodology, formal analysis, investigations, data curation, review and editing. S. C. L. D. conceptualization, formal analysis, investigations, writing, review and editing, funding. J. A. D. conceptualization, methodology, formal analysis, investigations, writing, review and editing, funding. All authors assisted in article revision, data interpretation and discussion of the results.

Availability of data and materials All data are included in the article or in the Supplementary Information.

Declarations

Ethical approval Not applicable.

Competing interests The authors declare no competing interests.

References

1. M. Misono, Heterogeneous catalysis of mixed oxides - perovskite and heteropoly catalysts. Stud. Surf. Sci. Catal. **176**, 97–151 (2013)
2. I.V. Kozhevnikov, Chem. Rev. **98**, 359 (1998). https://doi.org/10.1021/cr960400y
3. E. Rafiee, S. Eavani, RSC Adv. **6**, 46433 (2016). https://doi.org/10.1039/c6ra04891a
4. D.M. Ruiz, G.A. Pasquale, J.J. Martínez, G.P. Romanelli, Green Process. Synth. **11**, 766 (2022). https://doi.org/10.1515/gps-2022-0068

5. J. Haber, K. Pamim, L. Matachowski, B. Napruszewska, J. Poltowicz, J. Catal. **207**, 296 (2002). https://doi.org/10.1006/jcat.2002.3514
6. L. Matachowski, A. Drelinkiewicz, E. Lalik, M. Ruggiero-Mikołajczyk, D. Mucha, J.J. Krysciak – Czerwenka, Appl. Catal. A **469**, 290 (2014). https://doi.org/10.1016/j.apcata.2013.10.009
7. J. Gurgul, M. Zimowska, D. Mucha, R.P. Socha, L. Matachowski, J. Mol. Catal. A **351**, 1 (2011). https://doi.org/10.1016/j.molcata.2011.09.016
8. D. Zhao, J. Feng, Q. Huo, N. Melosh, G.H. Fredrickson, B.F. Chmelka, G.D. Stucky, Science **279**, 548–552 (1998). https://doi.org/10.1126/science.279.5350.54
9. H.I. Lee, J.H. Kim, G.D. Stucky, Y. Shi, C. Pak, J.M. Kim, J. Mater. Chem. **20**, 8483 (2010). https://doi.org/10.1039/C0JM00820F
10. V. Meynen, P. Cool, E.F. Vansant, Micropor. Mesopor. Mater. **125**, 170 (2009). https://doi.org/10.1016/j.micromeso.2009.03.046
11. M.R. Alves, M.F. Paiva, P.T.A. Campos, E.F. de Freitas, M.C.H. Clemente, G.A.V. Martins, A.T. Silveira, L.C.C. da Silva, M.C.A. Fantini, S.C.L. Dias, J.A. Dias, J. Porous Mater. **28**, 323 (2020). https://doi.org/10.1007/s10934-020-00994-x
12. A. Popa, V. Sasca1, O. Verdes, C. Ianasi, R. Banica (2017) J. Therm. Anal. Calorim. **127**:319. https://doi.org/10.1007/s10973-016-5534-3
13. J.M. Muller, G.C. Mesquita, S.M. Franco, L.D. Borges, J.L. Macedo, J.A. Dias, S.L. Dias, Micropor. Mesopor. Mater. **204**, 50 (2015). https://doi.org/10.1016/j.micromeso.2014.11.002
14. A.P.S. Dias, B. Rijo, M.F.CC. Pereira, R. Zăvoianu, O.D. Pavel, Reactions **5**, 260 (2024). https://doi.org/10.3390/reactions5010012.
15. B. Thangaraj, W. Monama, E. Mohiuddin, M.M. Mdleleni, Biores. Technol. **409**, 131230 (2024). https://doi.org/10.1016/j.biortech.2024.131230
16. T.K. Phung, L.P. Hernández, A. Lagazzo, G. Busca, Appl. Catal. A **493**, 77 (2015). https://doi.org/10.1016/j.apcata.2014.12.047
17. J. Zhou, N. Zhang, T. Meng, Q. Guo, Z. Xue, D. Mao, Nanomaterials **14**, 1558 (2024). https://doi.org/10.3390/nano14191558
18. P. Haro, P. Ollero, F. Trippe, Fuel Process. Technol. **114**, 35 (2013). https://doi.org/10.1016/j.fuproc.2013.03.024
19. S.D. Kim, S.C. Baek, Y. Lee, K. Jun, M.J. Kim, I.S. Yoo, Appl. Catal. A **309**, 139 (2006). https://doi.org/10.1016/j.apcata.2006.05.008
20. A. Jevremović, B.N. Vasiljević, A. Popa, S. Uskokovic-Markovic, L. Ignjatovic, D. Bajuk-Bogdanović, M.M. Rakic, Micropor. Mesopor. Mater. **315**, 110935 (2021). https://doi.org/10.1016/j.micromeso.2021.110925
21. I.H. Antunović, S.U. Marković, A. Popa, A. Jevremović, B.N. Vasiljević, M.M. Rakić, D. Bajuk-Bogdanović, Reac. Kinet. Mech. Cat. **128**, 121 (2019). https://doi.org/10.1007/s11144-019-01625-6
22. A. Popa, V. Sasca, O. Verdes, I.H. Antunović, Reac. Kinet. Mech. Catal. **115**, 355 (2015). https://doi.org/10.1007/s11144-015-0832-5
23. B. Viswanadham, V. Pavankumar, K.V.R. Chary, Catal. Lett. **144**, 744–755 (2014). https://doi.org/10.1007/s10562-014-1204-x
24. B. Viswanadham, N. Nagaraju, C.N. Rohitha, V. Vishwanathan, K.V.R. Chary, Catal. Lett. **148**, 397–406 (2018). https://doi.org/10.1007/s10562-017-2236-9
25. B. Viswanadham, A. Srikanth, K.V.R. Chary, J. Chem. Sci. **126**, 445–454 (2014). https://doi.org/10.1007/s12039-014-0586-z
26. B. Viswanadham, A. Srikanth, V.P. Kumar, K.V.R. Chary, J. Nanosci. Nanotechnol. **15**(7), 5391–5402 (2015). https://doi.org/10.1166/jnn.2015.9871
27. B. Viswanadham, J. Pedada, H.B. Friedrich, S. Singh, J. Mol. Catal. A Chem **425**, 116–123 (2016). https://doi.org/10.1016/j.molcata.2016.10.007
28. B. Viswanadham, V. Vishwanathan, K.V.R. Chary, Y. Satyanarayana, J. Porous Mater. **28**, 1269–1279 (2021). https://doi.org/10.1007/s10934-021-01070-8
29. B. Viswanadham, K.V.R. Chary, Catal. Lett. **152**, 2491–2497 (2022). https://doi.org/10.1007/s10562-021-03828-w
30. B. Viswanadham, V.D.B.C. Dasireddy, B. Putrakumarc, New J. Chem. **47**, 16897–16906 (2023). https://doi.org/10.1039/D3NJ02844E
31. B. Viswanadham, J. Chem. **2023**, 8888165 (2023). https://doi.org/10.1155/2023/8888165
32. A. Sakthivel, K. Komura, Y. Sugi, Ind. Eng. Chem. Res. **47**, 2538–2544 (2008). https://doi.org/10.1021/ie071314z

33. R. Yadav, T. Baskaran, A. Kaiprathu, M. Ahmed, S.V. Bhosale, S. Joseph, A.H. Al-Muhtaseb, G. Singh, A. Sakthivel, A. Vinu, Chem. Asian J. **15**, 2588–2621 (2020). https://doi.org/10.1002/asia.202000651
34. E.F. Freitas, M.F. Paiva, S.C.L. Dias, J.A. Dias, Catal. Today **289**, 70 (2017). https://doi.org/10.1016/j.cattod.2016.08.010
35. I. Holclajtner-Antunovic, D. Bajuk-Bogdanovic, A. Popa, V. Sasca, B.N. Vasiljevic, A. Rakic, S. Uskokovic-Markovic, Mater. Chem. Phys. **160**, 359 (2015). https://doi.org/10.1016/j.matchemphys.2015.04.052
36. C. Rocchiccioli-Deltcheff, M. Fournier, R. Franck, R. Thouvenot, Inorg. Chem. **22**, 207 (1983). https://doi.org/10.1021/ic00144a006
37. D. Mucha, L. Matachowski, T. Machej, J. Gurgul, R.P. Socha, Solid State Sci. **13**, 1276 (2011). https://doi.org/10.1016/j.solidstatesciences.2011.03.021
38. I.D. Holclajtner-Antunovic, A. Popa, D.V. Bajuk-Bogdanovic, S. Mentus, B.M.N. Vasiljevic, S.M., Uskokovic-Markovic. Inorg Chimica Acta **407**, 197 (2013). https://doi.org/10.1016/j.ica.2013.07.035
39. S. Zhu, X. Gao, F. Dong, Y. Zhu, H. Zheng, Y. Li, J. Catal. **306**, 155 (2013). https://doi.org/10.1016/j.jcat.2013.06.026
40. J.S. Santos, J.A. Dias, S.C.L. Dias, F.A.C. Garcia, J.L. Macedo, F.S.G. Sousa, L.S. Almeida, Appl. Catal. A **394**, 138 (2011). https://doi.org/10.1016/j.apcata.2010.12.034
41. H.P. Klug, L.E. Alexander, *X-Ray Diffraction Procedures for Polycrystalline and Amorphous Materials* (Wiley, New York, 1974), pp.491–538
42. I. Holclajtner-Antunovic, D. Bajuk-Bogdanovic, A. Popa, B.N. Vasiljevic, J. Krstic, S. Mentus, S. Uskokovic-Markovic, Appl. Surf. Sci. **328**, 466 (2015). https://doi.org/10.1016/j.apsusc.2014.12.062
43. J.A. Dias, E. Caliman, S.C.L. Dias, Micropor. Mesopor. Mater. **76**, 221 (2004). https://doi.org/10.1016/j.micromeso.2004.08.021
44. T. Okuhara, T. Nishimura, M. Misono, Stud. Surf. Sci. Catal. **101**, 581–590 (1996). https://doi.org/10.1016/S0167-2991(96)80269-2
45. E.P. Parry, J. Catal. **2**, 371 (1963). https://doi.org/10.1016/0021-9517(63)90102-7
46. C.F. Oliveira, L.M. Dezaneti, F.A.C. Garcia, J.L. deMacedo, J.A. Dias, S.C.L. Dias, K.S.P. Alvim, Appl. Catal. A **372**, 153 (2010). https://doi.org/10.1016/j.apcata.2009.10.027
47. F. Mariano-Neto, J.R. Matos, L.C.C. da Silva, L.V. Carvalho, K. Scaramuzzi, O.A. SantAnna, C.P. Oliveira, M.C.A. Fantini, J. Phys. D Appl. Phys. **47**, 425402 (2014). https://doi.org/10.1088/0022-3727/47/42/425402
48. M. Thommes, K. Kaneko, A.V. Neimark, J.P. Olivier, F. Rodriguez-Reinoso, J. Rouquerol, K.S.W. Sing, Pure Appl. Chem. **87**, 1051 (2015). https://doi.org/10.1515/pac-2014-1117
49. B. Aydemir, N.A. Sezgi, T. Doğu, AIChE J. **58**, 2466 (2012). https://doi.org/10.1002/aic.12763
50. D.W. Losito, D.R. Araujo, V.D.N. Bezzon, P.L.P. Filho, F.L.A. Fonseca, C.S. Chagas, E. Barbosa, C.L.P. Oliveira, M.C.A. Fantini, F.F. Ferreira, T.S. Martins, P.S. Haddad, A.C.S. Appl, Nano Mater. **4**, 13363 (2021). https://doi.org/10.1021/acsanm.1c02861
51. D. Varisli, T. Dogu, G. Dogu, Chem. Eng. Sci. **62**, 5349 (2007). https://doi.org/10.1016/j.ces.2007.01.017
52. L. Matachowski, M. Zimowska, D. Mucha, T. Machej, Appl. Catal. B **123**, 448 (2012). https://doi.org/10.1016/j.apcatb.2012.05.003
53. M. Mokhtar, S.N. Basahel, T.T. Ali, J. Ind. Eng. Chem. **20**, 46 (2014). https://doi.org/10.1016/j.jiec.2013.04.028
54. W. Trakarnpruk, Mendeleev Commun. **23**, 168 (2013). https://doi.org/10.1016/j.mencom.2013.05.017
55. D.S. Valadares, J.O.C. deFrança, R.C. Fernandes, L.M. Dezaneti, S.C.L. Dias, J.A. Dias, Chemistry **5**, 1138 (2023). https://doi.org/10.3390/chemistry5020078
56. A. Zieba, L. Matachowski, J. Gurgul, E. Bielanska, A. Drelinkiewicz, J. Mol. Catal. A **316**, 30 (2010). https://doi.org/10.1016/j.molcata.2009.09.019
57. M.E. Manriquez, T. Lopez, R. Gomez, J. Navarrete, J. Mol. Catal. A **220**, 229 (2004). https://doi.org/10.1016/j.molcata.2004.06.003
58. A. Zhukova, S. Chuklina, Y. Fionov, N. Vakhrushev, A. Sazonova, I. Mikhalenko, D. Zhukov, O. Isaikina, A. Fionov, A. Il'icheva, Res. Chem. Intermed. **50**, 1331 (2024). https://doi.org/10.1007/s11164-023-05174-5

59. M. Ngcobo, P.R. Makgwane, M.K. Mathe, Appl. Catal. O **193**, 206976 (2024). https://doi.org/10.1016/j.apcato.2024.206976
60. P.L.A. Coutinho, A.T. Morita, L.F. Cassinelli, A. Morschbacker, W. doCarmo, *Catalytic Process Development for Renewable Materials* (Wiley, Hoboken, 2013), pp.149–165. https://doi.org/10.1002/9783527656639.ch6
61. A. Galadima, O. Muraza, J. Ind. Eng. Chem. **31**, 1 (2015). https://doi.org/10.1016/j.jiec.2015.07.015
62. D. Fan, D.-J. Dai, H.-S. Wu, Materials **6**, 101 (2013). https://doi.org/10.3390/ma6010101

Authors and Affiliations

Mayara A. Resende[1] · Maria Clara Hortencio Clemente[1] · Gesley Alex Veloso Martins[1] · Luís Carlos Cides da Silva[2] · Marcia C. A. Fantini[2] · Sílvia C. L. Dias[1] · José A. Dias[1]

✉ José A. Dias
jdias@unb.br; josediasunb@gmail.com

Mayara A. Resende
res.may91@gmail.com

Maria Clara Hortencio Clemente
mrclara01@gmail.com

Gesley Alex Veloso Martins
gesley@gmail.com

Luís Carlos Cides da Silva
luiscides@gmail.com

Marcia C. A. Fantini
mfantini@if.usp.br

Sílvia C. L. Dias
scdias@unb.br

[1] Universidade de Brasília, Instituto de Química - Laboratório de Catálise (A1-62/21), Campus Darcy Ribeiro, Asa Norte, Brasília, DF 70910-900, Brazil

[2] Instituto de Física, Universidade de São Paulo, Cidade Universitária, Rua Do Matão Nº 1371, São Paulo, SP 05508-090, Brazil